Kobe University Repository : Kernel

PDF issue: 2025-12-05

Timing of the faulting on the Wispy Terrain of Dione based on stratigraphic relationships with impact craters

Hirata, Naoyuki

(Citation)
Journal of Geophysical Research: Planets,121(11):2325-2334

(Issue Date)
2016-11

(Resource Type)
journal article

(Version)
Version of Record

(Rights)
©2016 American Geophysical Union

(URL)
https://hdl.handle.net/20.500.14094/90003880

KOBE UNIVERSITY

AGU PUBLICATIONS

JGR

Journal of Geophysical Research: Planets

RESEARCH ARTICLE
10.1002/2016JE005176

Key Points:
- Stratigraphic relationships between faults and impact craters were applied to determine the timing of the faulting
- The paucity of superposed craters implies that the faulting is 0.30–0.79 Ga
- This indicates that the faulting of the Wispy Terrain on Dione is a very recent event

Supporting Information:
- Supporting Information S1
- Figure S1
- Figure S2
- Figure S3
- Figure S4
- Figure S5
- Figure S6
- Figure S7
- Figure S8
- Figure S9
- Figure S10
- Figure S11
- Figure S12
- Figure S13
- Figure S14
- Figure S15
- Figure S16
- Figure S17

Correspondence to:
N. Hirata,
hirata@tiger.kobe-u.ac.jp

Citation:
Hirata, N. (2016), Timing of the faulting on the Wispy Terrain of Dione based on stratigraphic relationships with impact craters, *J. Geophys. Res. Planets*, *121*, 2325–2334, doi:10.1002/2016JE005176.

Received 25 MAR 2016
Accepted 31 OCT 2016
Accepted article online 7 NOV 2016
Published online 22 NOV 2016

©2016. American Geophysical Union. All Rights Reserved.

Timing of the faulting on the Wispy Terrain of Dione based on stratigraphic relationships with impact craters

Naoyuki Hirata[1]

[1]Graduate School of Science, Kobe University, Kobe, Japan

Abstract The trailing hemisphere of Dione is characterized by the Wispy Terrain, where it exhibits a hemispheric-scale network of extensional tectonic faults superposed on the moon's cratered surface. The faults likely reflect past endogenic activity and Dione's interior thermal history. Although fresh exposures of pristine scarps indicate that the timing of the faulting is relatively recent, the absolute age of the faulting remains uncertain. To estimate the timing of the faulting, we investigated stratigraphic relationships between impact craters and faults. Using high-resolution images obtained by the ISS camera onboard the Cassini spacecraft, we investigated craters with diameters exceeding or equal to 10 km that coincide spatially with the faults and classified the craters as crosscut craters or superposed craters. As a result, at least 82% of the craters were interpreted as clear examples of crosscut craters and 12% of the craters were interpreted to be candidates of superposed craters, although stratigraphic relationships are often ambiguous. The paucity of superposed craters and a predicted cratering rate indicate that the faulting of the Wispy Terrain is 0.30–0.79 Ga. If 12–18% of the craters are assumed to be superposed, the timing of the faulting could be in the range 0.30–0.79 Ga. However, it is possible that the faulting of the Wispy Terrain is still ongoing.

1. Introduction

Tectonic structures are prominent on Dione, and analyses of the faults can provide insight into its geologic history. Dione, with a radius of 561 km, is a midsized satellite in the Saturn system. Dione is Saturn's third densest moon, and its silicate mass fraction is estimated to be 50% [*Matson et al*., 2009; *Thomas et al*., 2007]. Radioactivity from the high amount of internal silicate material provided heat to Dione's interior and likely contributed to prolonged endogenic activity [*Consolmagno and Lewis*, 1978; *Hillier and Squyres*, 1991; *Moore*, 1984]. For example, tectonic fault systems in the Wispy Terrain (Figure 1a) are suggested to be relatively young geologic features [*Kirchoff and Schenk*, 2015; *Stephan et al*., 2010], although the timing of the faulting is still uncertain. To constrain the timing, we analyzed stratigraphic relationships between faults and craters.

The Wispy Terrain, defined as the area containing tectonic fault systems, mostly covers Dione's trailing hemisphere. A network of bright linear features on Dione's trailing hemisphere (Figure 1a), called the wispy streaks or wispy markings, was first discovered during the Voyager flybys [*Smith et al*., 1981; *Smith et al*., 1982] and interpreted as bright exposures along troughs formed by either extensional tectonics [*Moore*, 1984; *Plescia and Boyce*, 1982] or cryovolcanism [*Plescia*, 1983; *Stevenson*, 1982]. Higher-resolution images, obtained by the ISS camera onboard the Cassini spacecraft (Figure 1b), revealed that these bright linear features are sets of subparallel grabens with interstitial horsts in some regions [*Wagner et al*., 2006]. The presence of these grabens and horsts are indicative of normal faulting induced by extensional tectonism [e.g., *Jaumann et al*., 2009; *Stephan et al*., 2010; *Wagner et al*., 2006]. The fault scarp of Padua Chasmata has a slope of ~23°, which is shallower than expected from laboratory deformation experiments; so modifications such as viscous relaxation have been suggested to explain such shallow slopes [*Beddingfield et al*., 2015]. The existence of many polygonal impact craters in the Wispy Terrain implies that numerous subtle or nonvisible fractures extend across the surface of Dione [*Beddingfield et al*., 2016].

The fault scarps of the Wispy Terrain are relatively fresh; high-resolution images (for example, Figure 1c) indicate that slopes of the scarps show a paucity of landforms associated with mass wasting or erosion caused by impact cratering. This view received further support from *Stephan et al*. [2010], who found that the fault scarps expose clean H_2O ice. This fresh exposure implies that formation of the fault scarps could have

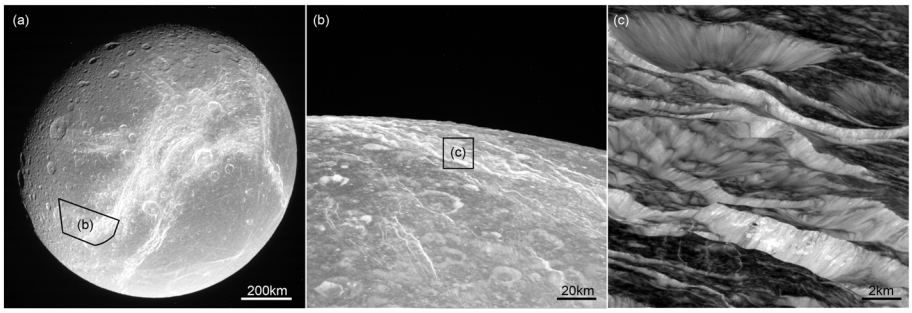

Figure 1. (a) Dione's trailing hemisphere (N1532405095). (b) A close-up view of the fault scarps of the Wispy Terrain (W1649311515). (c) One of the highest-resolution images of the faults (N1649311515; 14 m/pixel). Insets outline the locations of Figures 1b and 1c.

continued into a relatively recent time. However, such fresh exposure may alternatively be explained by recent small downslope movements. If so, the main faulting may be much older.

Kirchoff and Schenk [2015] estimated the age of the Wispy Terrain to be ~2.5 Ga based on crater density. Similarly, *Wagner et al*. [2006] estimated the age of the Wispy Terrain to be either older than 3.7 Ga or older than 1 Ga. However, these estimated ages are applicable to only the underlying surface and not applicable to the faulting itself [*Kirchoff and Schenk*, 2015; *Stephan et al*., 2010], because these researchers did not evaluate whether each impact crater was formed after or before the faulting. As both of these studies proposed, the faults should be younger than the Wispy Terrain.

2. Data and Methods

We investigated the stratigraphic relationships between faults and craters to better constrain the fault ages. We used the methodology applied to faults on the Moon and Mercury [e.g., *Banks et al*., 2015; *Byrne et al*., 2014; *Watters et al*., 2012]. Such studies commonly examine crosscut craters and superposed craters on fault scarps. They assume that a crater crosscut by scarps is formed before the faulting and that a crater superposed on scarps is formed after the faulting. We investigated impact craters that coincide spatially with the faults of the Wispy Terrain in addition to the superposition relationships between impact craters and faults.

2.1. Cassini Images

We used 95 images obtained by eight close encounters of the Cassini spacecraft (orbits B, 16, 50, 98, 137, 165, 214, and 217) (Table 1 and Figure 2a). A complete list of the images is included as supporting information Table S1. The fault systems of the Wispy Terrain are divided into six units: Carthage Fossae (CA), Clusium Fossae (CL), Palatine Chasmata (PL), Eurotas Chasmata (EU), Aurunca Chasmata (AU), and Padua Chasmata (PD) (Figure 2b) [*Jaumann et al*., 2009; *Roatsch et al*., 2009]. The images cover almost all of the fault systems of the Wispy Terrain, except for the west end of PL, at a resolution of 25 m/pixel to 700 m/pixel (Figures 2c and 2d). We focused on craters with diameters larger than 10 km ($D_c \geq 10$ km), which would be at least 20 pixels across the images used, to assure that the evaluation of the stratigraphic relationships was not strongly affected by image resolution, although classification of larger craters would be more reliable. We did not consider craters with diameters smaller than 10 km ($D_c < 10$ km). Note that D_c stands for crater diameter.

Table 1. The Eight Close Flyby Orbits Used in This Work

Orbit	Date	Number of Images	Resolution (m/pixel)
B	15 Dec 2004	4	432
16	12 Oct 2005	19	25–360
50	30 Sep 2007	13	272–415
98	7 Apr 2010	10	115–353
137	4 Sep 2010	17	235–304
165	3 May 2012	9	170–474
214	11 Apr 2015	6	660
217	16 Jun 2015	13	437–522

2.2. Crater Classification

We classified all craters coinciding spatially with the faults into four types based on the intersection between crater and fault scarps (Table 2 and Figure 3). A Type A crater is a crater in which fault

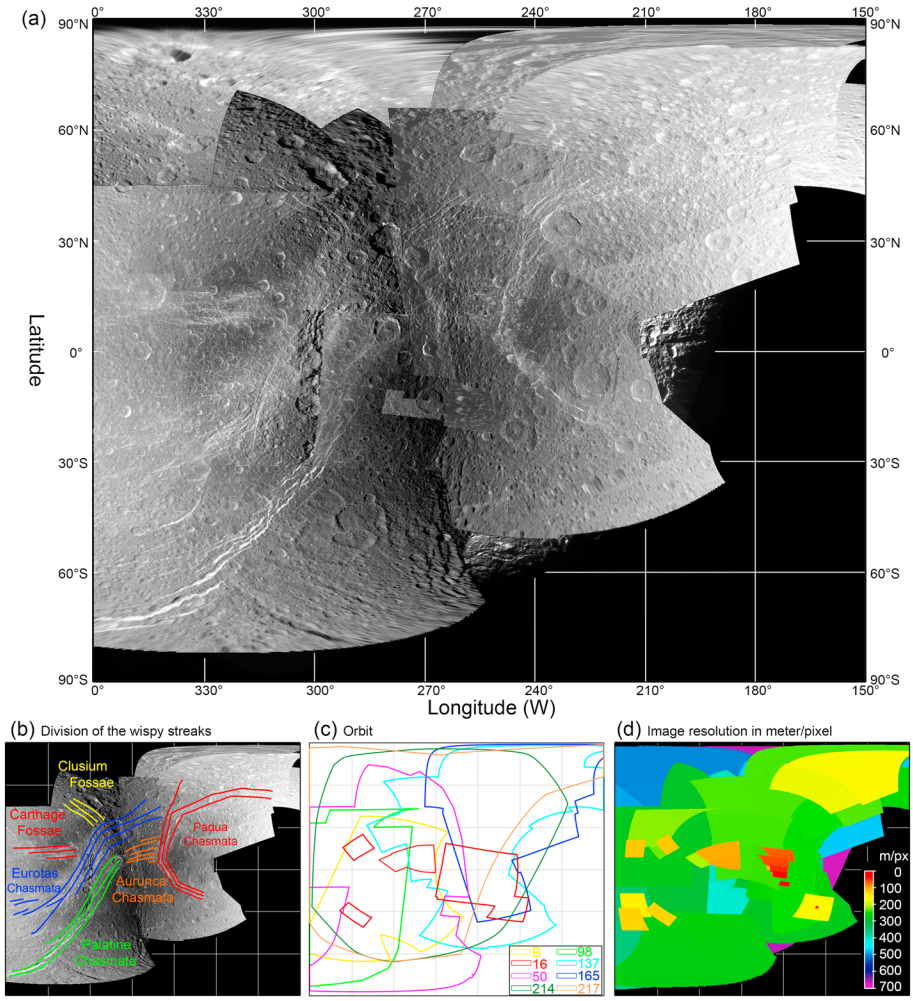

Figure 2. (a) Hemispheric mosaic of the Wispy Terrain in simple cylindrical projection. (b) Nomenclature for each division of the fault system. (c) The regions imaged in each orbit. (d) The image resolution for each location in m/pixel. Red indicates higher resolution, and blue indicates lower resolution. The base maps of Figures 2b–2d are equivalent to the map in Figure 2a.

scarps can be identified on the crater floor. A Type B crater has identifiable fault scarps on the rim crest and inner wall of the crater, but not on the floor. A Type C crater has fault scarps adjacent to the crater, but not on the floor or the inner wall of the crater, and a Type D crater is a crater that is unrelated to the faults (i.e., the crater is sufficiently far from the nearest faults). We defined Types A, B, and C as impact craters coinciding spatially with the faults. Although most of the craters on the Wispy Terrain are Type D craters, it is impossible to evaluate their superposition relationships, so we do not discuss Type D craters further.

Because the floor of a crater is generally filled by a breccia lens [*Grieve et al*., 1989; *Melosh*, 1989], we considered Type A craters to be clear examples of craters formed before the faulting. On the other hand, the superposition of Type B craters could be uncertain for the following reasons. Many of the grabens on the Wispy Terrain are often faint (or not visible in available images) at topographic lows (Figure 4), presumably because the depth of each fault is typically shallower than surface undulations. Following structural analyses of lunar grabens [*Golombek*, 1979; *McGill*, 1971] and assuming the width and the dip of the faults within a typical graben of the Wispy Terrain to be 5 km and 23° (the dip obtained by *Beddingfield et al*. [2015]), the base of the faulted layer is at the depth of 1 km, which is less than the depth of the craters. Based on this argument, most of the Type B craters are examples of craters formed before the faulting. However, Type B craters may be craters formed after the faulting because faults on an inner crater wall could be preexisting faults exposed by the collapse of a transient crater wall. Type C craters are candidates for craters that formed after the faulting.

Table 2. Crater Classification and Interpretation of This Work

Crater Type	Definition	Superposition
Type A	A crater in which fault scarps can be identified on the crater floor	Before the faulting
Type B	A crater which has identifiable fault scarps on the rim crest and inner wall of the crater, but not on the floor	Before or after the faulting
Type C	A crater which has fault scarps adjacent to the crater, but not on the floor or the inner wall of the crater	After the faulting
Type D	A crater unrelated to the faults (i.e., the crater is sufficiently far from the nearest faults)	Uncertain

However, some Type C craters may have formed before the faulting because even Type C craters could be alternatively explained by an ejecta blanket that sufficiently obscures faults near the crater rim.

Generally, in the case of the Moon or Mars, the extent of a continuous ejecta blanket is effective for stratigraphic classification because the thickness of the ejecta blanket is sufficient to obscure preexisting grabens [e.g., *Kneissl et al*., 2015; *Smith et al*., 2009]. On the other hand, ejecta blankets of craters on Dione generally have insufficient thickness to obscure preexisting faults presumably because the low gravity of Dione allows ejecta to travel much farther from the impact site. In fact, it is known that only a few craters have recognizable ejecta blankets on Dione [*Plescia*, 1983]. Therefore, to obtain a correct stratigraphic classification, we examined the rim crest and the floor of each crater and did not rely on ejecta blankets.

Note that the visibility of fault scarps also depends on the illumination or resolution of the images. For example, the three images in Figure 5 show the same impact crater in orbits 50, 137, and B (from left to right) projected at the same scale and the same projection. Orbits 50 and 137 did not image scarps on the crater floor or inner wall due to shadow and illumination. Therefore, a crater in the center of the figure would be classified as Type C if the classification was based on the image of orbit 50 or 137, but it would be Type A if based on the three images. Thus, a Type C crater could actually be a Type A or B crater, and a Type B crater could be a Type A. Because of the reasons mentioned in this subsection, this type of classification or stratigraphic interpretation is often ambiguous.

2.3. Identification and Measurements

Impact craters were identified by the existence of a circular, elliptical, or polygonal depression. The fault scarps were determined by linear slopes where bright material has been exposed, possibly due to normal faulting. The identifications were assessed by using the eight flyby images and the digital elevation model developed by *Gaskell* [2013] (Figure 6). The flyby images provide different illumination of the Wispy Terrain and were useful for understanding the surface undulations, such as faults and craters. For example, the solar incidence during the flyby of orbit B brightened the east facing slopes of the craters or scarps of PL and EU, whereas the incidence during the flybys of orbits 50 and 90 brightened the west facing slopes of PL and EU. Most of the faults of the Wispy Terrain were covered by images from more than two flybys. Moreover, the digital elevation models of Dione with a spatial resolution of approximately 1.5 km, developed by *Gaskell* [2013], were used to improve the identification of scarps and crater depressions. The interpretations are organized in sketch maps (supporting information Figures S1–S3).

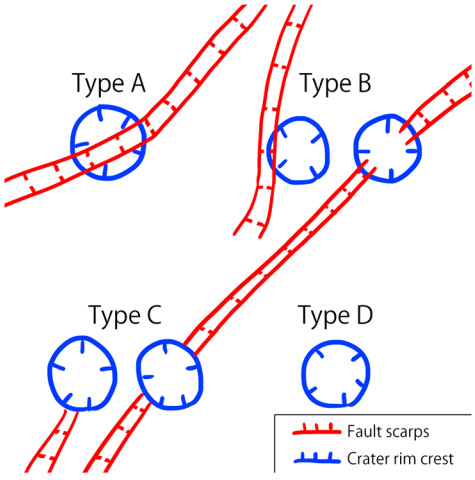

Figure 3. The definition of the classification of this work. A Type A crater is a crater with its floor cut by faults, a Type B crater is a crater with its inner wall but not its floor cut by faults, a Type C crater is a crater with an inner wall and floor not cut by faults, and a Type D crater is a crater sufficiently far from the nearest faults.

The Integrated Software for Imagers and Spectrometers (ISIS3), produced by the U.S. Geological Survey, was used to calibrate the Cassini images.

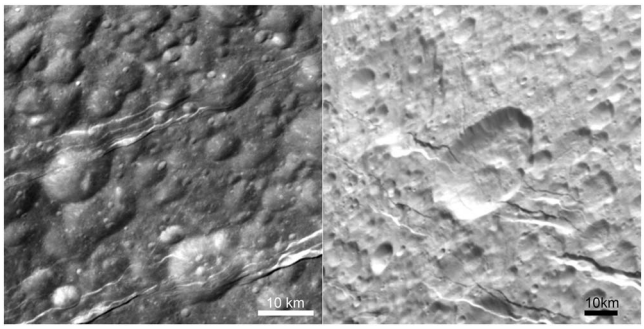

Figure 4. Faults scarps of the Wispy Terrain. Many of the grabens on the Wispy Terrain are faint or not visible in topographic lows ((left) N1649313734 and (right) N1662201249).

To measure the diameters and the locations of impact craters, this investigation utilized the Java Mission-planning and Analysis for Remote Sensing (JMARS) program produced by Arizona State University. The craters were measured from the maps shown in Figure 2a.

3. Results

We identified 387 examples of craters coinciding spatially with the faults. The diameters, locations, and types of all the craters are shown in supporting information Table S2. For craters ($D_c \geq 10$ km), 82% of the total are Type A, 6% are Type B, and 12% are Type C (Table 3).

Craters classified as Type C, with diameters larger than 25 km, are shown in Figure 7. Although the rims and walls of the six craters are not cut by faults, there are small-scale faults adjacent to the craters but no faults on the opposite side of the craters. Thus, it is likely that the surrounding faults did not reach beyond the crater rim crests when the faults formed. Because most of the Type C craters with 25 km $> D_c \geq 10$ km are similar to these examples, craters formed after the faulting may be limited to only a small fraction of Type C craters. Complete illustrations for all craters (Types A, B, and C) are included in supporting information Figures S4–S17. Note that some of the craters smaller than 10 km provide reliable examples of craters superposed on faults (Figure 8), although we do not discuss these craters in detail.

4. Discussion

For age determination of the linear surface features, we followed the ideas developed by many authors [e.g., *Kneissl et al*., 2015; *Smith et al*., 2009; *Tanaka*, 1982; *Wichman and Schultz*, 1989]. These ideas assume that the area to use to obtain the crater number density is defined by the area enclosed by one crater radius away from the linear features (in this case, the faults) (Figure 9). If the linear features are sparsely distributed and the length of the linear features (L) is sufficiently longer than either one crater radius (r) or the width of the linear features, the area (A) is simply determined by $A(r) = 2Lr$.

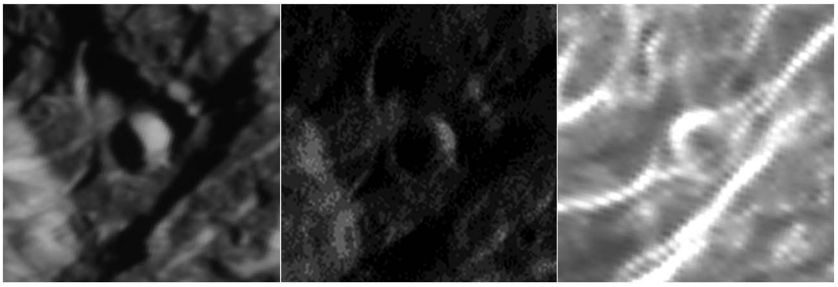

Figure 5. Example comparison among images from orbits 50, 137, and B (from left to right, respectively). The three images show the same impact crater (with a diameter of 7.61 km) centered at 13.2°N, 284.8°W and are shown at the same scale.

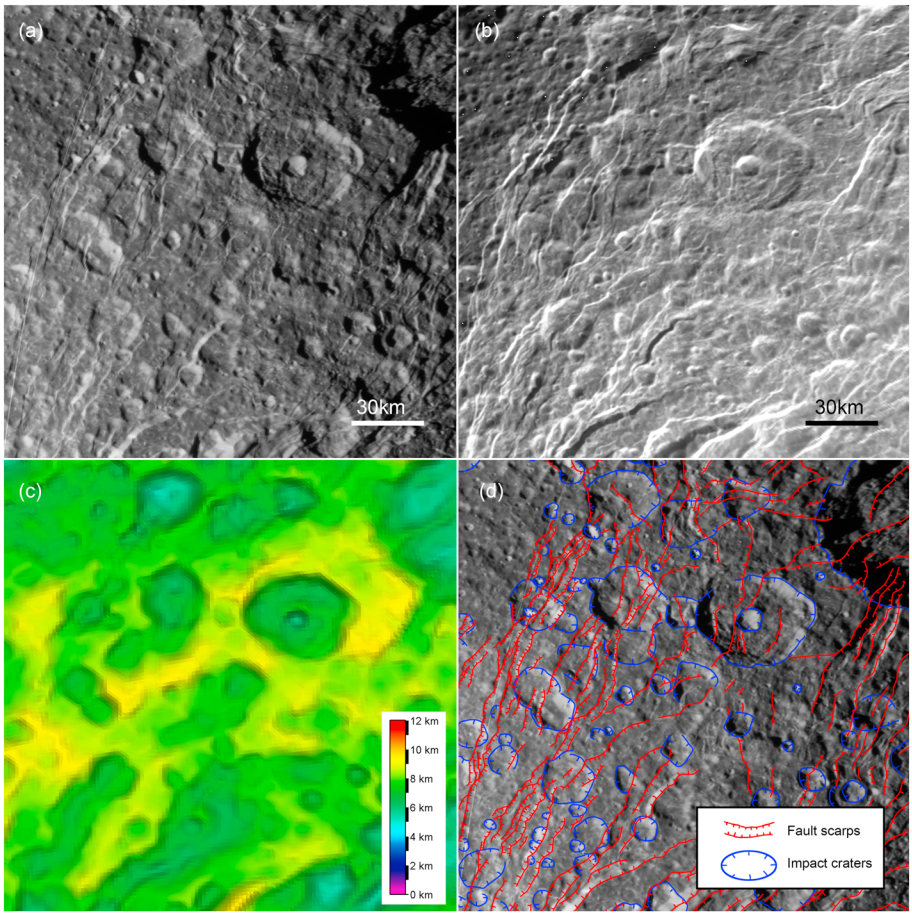

Figure 6. Example of the identification of the impact craters and the fault scarps of Eurotas Chasmata. The base map is centered at 292.1°W and 22.3°N, and its projection is simple cylinder. (a) Images in orbit 50. (b) Images in orbit B. (c) Topography from *Gaskell* [2013]. (d) Sketch map of the craters (blue lines) and the fault scarps (red lines) based on the investigation. The hachures point downscarp, and the lines without hachures indicate that the downscarp direction is uncertain.

However, because the faults of the Wispy Terrain are densely distributed, we needed to compute the value of $A(r)$ numerically. Based on the mapping of the fault systems (supporting information Figures S1–S3), the area enclosed by the radius r (km) from the fault systems of the Wispy Terrain is approximated well by the equation

$$A(r) = 9370.79r + 557653 - 1180990/r \quad \left(\mathrm{km}^2\right). \tag{1}$$

Following *Tanaka* [1982], the crater number density (N_c) can be extrapolated by the sum of the individual counts:

$$N_c = \Sigma_{i=1}^{k} \frac{1}{A(r_i)} \quad \left(\mathrm{km}^{-2}\right), \tag{2}$$

where r_i is the radius of the ith crater and $i = \{1, \ldots, k\}$ are defined by all craters larger than a given size.

Table 3. The Number of Each Type of Craters

	Type A	Type B	Type C	Total
$D_c \geq 50$ km	13	1	0	14
$D_c \geq 30$ km	37	3	3	43
$D_c \geq 20$ km	100	4	12	116
$D_c \geq 10$ km	316	23	48	387

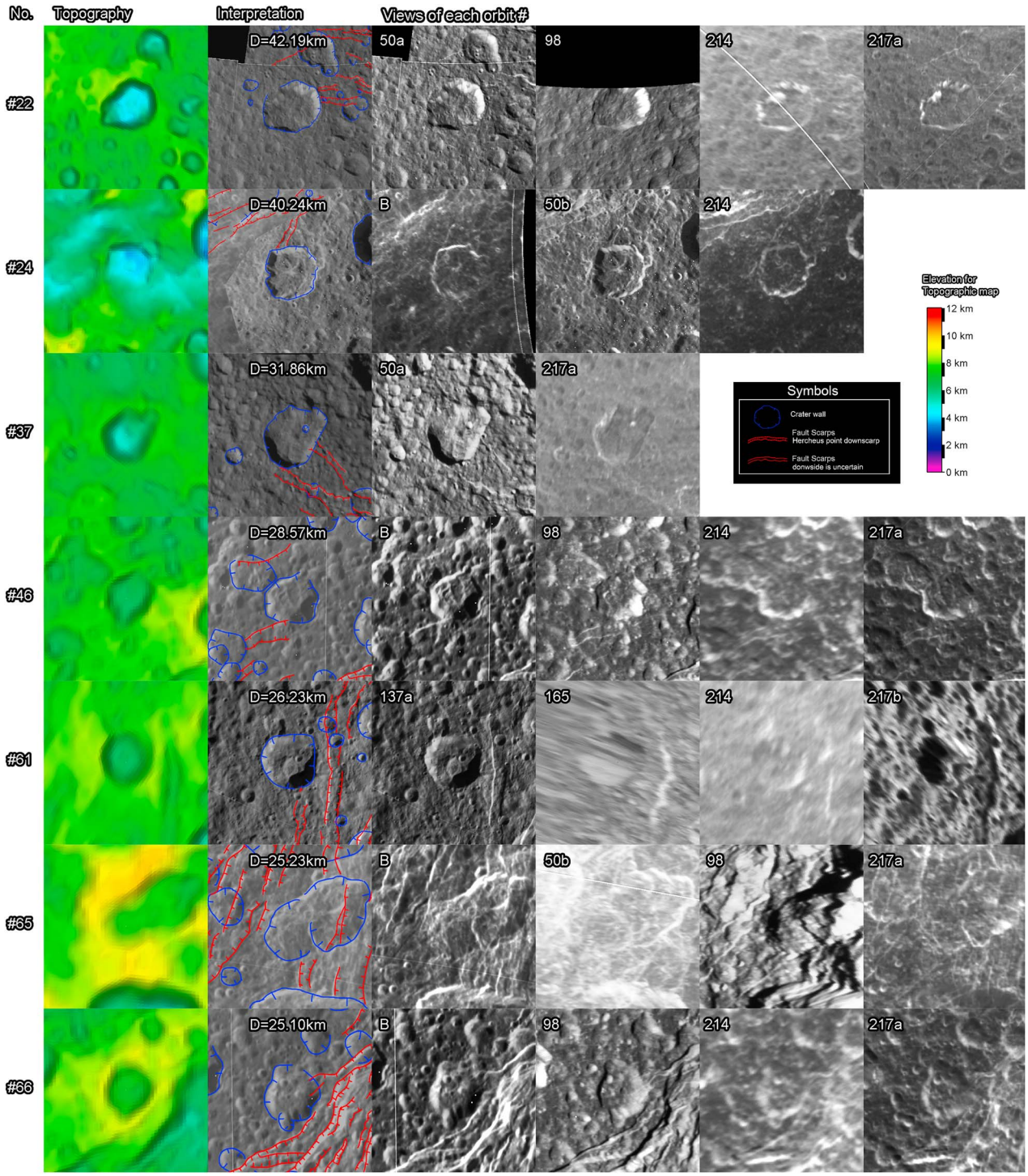

Figure 7. Type C craters with diameter larger than 25 km. Images shown in the same line are of the same crater projected in the same geometry; azimuthal equidistant projection centered at the crater (each crater's longitude and latitude are shown in Table S2). The ground scale is set so that each crater diameter is one third of the width of each image. The numbers at the left correspond to the crater numbers in Table S2. The left end column shows the topography (its elevation scale is shown in the top right of this figure), the second column from the left shows the interpretation of the faults and the craters in this work (its symbol is shown in the upper right), and the third and subsequent columns from the left to the right are mosaics merged from images obtained by the Cassini flybys. The other craters are shown in supporting information Figures S4–S17.

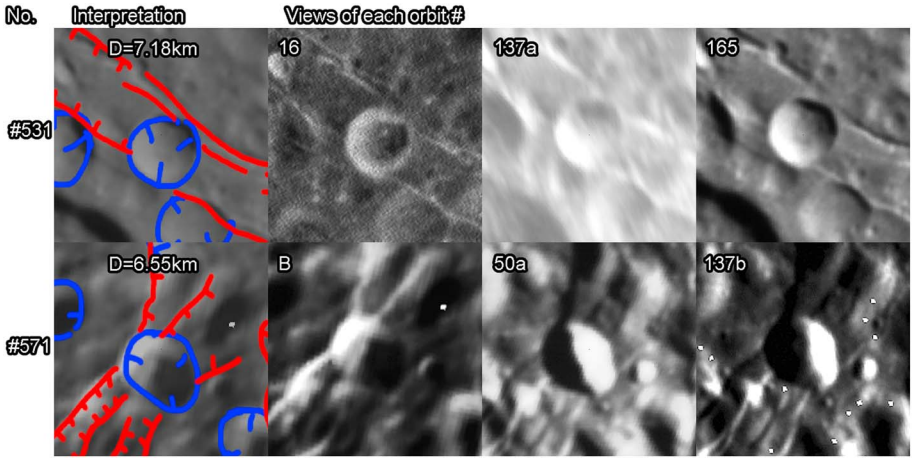

Figure 8. Candidates of superposed craters on faults. The left end column shows the interpretation of faults and craters in this work, and the second and subsequent columns from left to right are mosaics merged from images obtained by the Cassini flybys.

The heliocentric cratering rate was estimated theoretically by *Zahnle et al*. [2003]. Because of the uncertainty of the cratering rate in the outer solar system, they defined two cases: Case A, which is extrapolated from the cratering rate in the Jovian system, and Case B, which is extrapolated from the cratering rate for Triton. Thus, the theoretical cratering rate (R_A and R_B) for craters larger than a given crater diameter (D_c) on Dione is given by

$$R_A = 3.0\times10^{-14}\left(\frac{D_c}{10}\right)^{-1.277} \left(\text{ km}^{-2} \text{ yr}^{-1} \right) \text{ for Case A or} \tag{3}$$

$$R_B = 1.9\times10^{-13}\left(\frac{D_c}{10}\right)^{-2.171} \left(\text{ km}^{-2} \text{ yr}^{-1} \right) \text{ for Case B.} \tag{4}$$

We dated the fault systems using equations (2)–(4).

If we assume that Type A craters are crosscut craters and that Types B and C craters are superposed craters, the crater number density for superposed craters ($D_c \geq 10$ km) is 149.28 craters/10^6 km^2. Thus, the age of the faulting is estimated to be 5.0 Gyr in Case A and 0.79 Gyr in Case B. If we assume that Types A and B are crosscut craters and that Type C is superposed craters, the crater number density for the superposed craters ($D_c \geq 10$ km) is 101.67 craters/10^6 km^2. Thus, the age of the faulting is estimated to be 3.4 Gyr in Case A and 0.54 Gyr in Case B. If the timing of the faulting is estimated to be 18% (Types B and C) or 12% (only Type C) of 2.5 Ga, it would be 0.45 Ga or 0.30 Ga, respectively. Considering the existence of Type A craters (82% of the total) and the age of the Wispy Terrain (~2.5 Ga) determined by *Kirchoff and Schenk* [2015], the age based on Case A is unlikely. Overall, the timing of the faulting is estimated to be between 0.30 and 0.79 Ga. Those estimated ages are organized into Table 4. Considering that most Type C craters are not very clear examples of superposed craters, the timing of the faulting may be much younger than the age obtained. Therefore, the possibility that the faulting is an ongoing event cannot be ruled out.

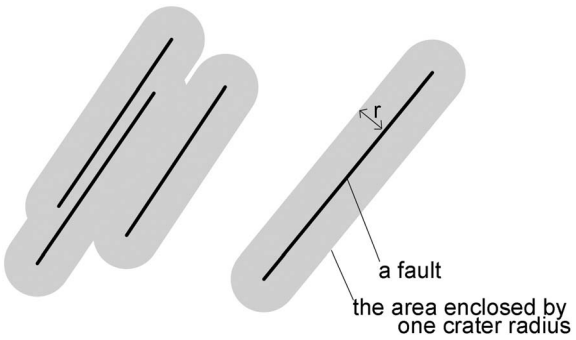

Figure 9. The concept of the definition of area to obtain crater density. The gray regions enclosed by a given radius (r) from a fault are equivalent to $A(r)$ in equation (1).

Note that it is unlikely that the ages of these faults are the same, and each unit of the fault systems could have

Table 4. The Estimated Age of the Faulting

Assumption	Case A	Case B	Other[a]
If Type A is crosscut while Type B and C are superposed	5.0 Gyr	0.79 Gyr	0.45 Gyr
If Type A and B are crosscut while Type C is superposed	3.4 Gyr	0.54 Gyr	0.30 Gyr

[a]Based on the age of the Wispy Terrain (2.5 Gyr) and the fraction of crosscut craters out of the total craters.

a variant age. In other word, the faulting may occur as multiple events, rather than a single event. Furthermore, the possibility of faults being reactivated cannot be ruled out, and therefore, craters superposed on faults at its formation may be cut by the reactivation of faults. If so, some of crosscut craters would reflect the timing of the reactivation instead. Therefore, the timing of the faulting obtained could be said to be the averaged value of all faults. In any case, the timing of the faulting of the Wispy Terrain is quite recent, possibly even ongoing. However, the stratigraphic relationships are ambiguous, as discussed in section 2.2; therefore, this method involves uncertainty.

Some of the crosscut craters in this study would be reclassified as superposed craters by other researchers. If 5% of the Type A craters were reclassified as superposed craters, the age would be 0.18 Gyr older than the original dating. Additional work on the stratigraphic relationship between the dark terrain and the faults of the Wispy Terrain may provide a more reliable age for the faulting. It is known that the faults of the Wispy Terrain are superposed on the dark surface of the trailing hemisphere [*Stephan et al*., 2010], and the dark surface is considered to be the result of the accumulation of dark materials during the last 1–50 Ma [*Hirata and Miyamoto*, 2016]. Interestingly, this age is consistent with this work.

5. Conclusion

More than 387 impact craters ($D_c \geq 10$ km) coinciding spatially with the fault system of the Wispy Terrain were identified and classified as crosscut craters or superposed craters based on geological investigation. As a result, we interpreted that at least 82% of the total craters examined are reliable examples of crosscut craters and that the rest are candidates of superposed craters. Based on the theoretical cratering rate, the fault ages are between 0.30 and 0.79 Ga. This indicates that the faulting is a very recent event. On the other hand, stratigraphic relations are often ambiguous, and the detailed timing and accuracy of this type of study remain unclear. For example, if 5% of the Type A craters were reclassified as superposed crates, the age would be 0.18 Gyr older than the original dating. Further studies, such as studies on the stratigraphic relationship between the dark surface of the trailing hemisphere and the faults of the Wispy Terrain, may provide a more reliable timing for the faulting.

Acknowledgments
The author thanks Chloe Beddingfield, Michelle Kirchoff, and Noah Hammond for their helpful comments and suggestions, which significantly improved this work. This work was supported by a Grant-in-Aid for JSPS Fellows. The image data (http://pds.nasa.gov) and the shape model of Dione (http://sbn.psi.edu/pds/asteroid/) are freely available via NASA's Planetary Data System. The software ISIS3 (http://isis.astrogeology.usgs.gov/) and JMARS (https://jmars.asu.edu/) were used in this work.

References

Banks, M. E., Z. Xiao, T. R. Watters, R. G. Strom, S. E. Braden, C. R. Chapman, S. C. Solomon, C. Klimczak, and P. K. Byrne (2015), Duration of activity on lobate-scarp thrust faults on Mercury, *J. Geophys. Res. Planets*, *120*, 1751–1762.

Beddingfield, C. B., D. M. Burr, and W. M. Dunne (2015), Shallow normal fault slopes on Saturnian icy satellites, *J. Geophys. Res. Planets*, *120*, 2053–2083, doi:10.1002/2015JE004852.

Beddingfield, C. B., D. M. Burr, and L. T. Tran (2016), Polygonal impact craters on Dione: Evidence for tectonic structures outside the Wispy Terrain, *Icarus*, *274*, 163–194, doi:10.1016/j.icarus.2016.03.020.

Byrne, P. K., C. Klimczak, A. M. Celal Sengor, S. C. Solomon, T. R. Watters, and S. A. Hauck II (2014), Mercury's global contraction much greater than earlier estimates, *Nat. Geosci.*, *7*(4), 301–307, doi:10.1038/ngeo2097.

Consolmagno, G. J., and J. S. Lewis (1978), The evolution of icy satellite interiors and surfaces, *Icarus*, *34*(2), 280–293.

Golombek, M. P. (1979), Structural analysis of lunar grabens and the shallow crustal structure of the Moon, *J. Geophys. Res.*, *84*(B9), 4657–4666, doi:10.1029/JB084iB09p04657.

Gaskell, R. W. (2013), Gaskell Dione Shape Model V1.0. CO-SA-ISSNA/ISSWA-5-DIONESHAPE-V1.0. NASA Planetary Data System. [Available at http://sbn.psi.edu/pds/resource/dioneshape.html.]

Grieve, R. A. F., J. B. Garvin, J. M. Coderre, and J. Rupert (1989), Test of a geometric model for the modification stage of simple impact crater development, *Meteoritics*, *24*(2), 83–88, doi:10.1111/j.1945-5100.1989.tb00948.x.

Hillier, J., and S. W. Squyres (1991), Thermal stress tectonics on the satellites of Saturn and Uranus, *J. Geophys. Res.*, *96*(E1), 15,665–15,674, doi:10.1029/91JE01401.

Hirata, N., and H. Miyamoto (2016), Rayed craters on Dione: Implication for the dominant surface alteration process, *Icarus*, *274*, 116–121, doi:10.1016/j.icarus.2016.03.021.

Jaumann, R., R. N. Clark, F. Nimmo, A. R. Hendrix, B. J. Buratti, T. Denk, J. M. Moore, P. M. Schenk, S. J. Ostro, and R. Srama (2009), Icy satellites: Geological evolution and surface processes, in *Saturn From Cassini-Huygens*, edited by M. K. Doughherty, L. W. Esposito, and S. M. Krimigis, pp. 637–681, Springer, Netherlands.

Kirchoff, M. R., and P. Schenk (2015), Dione's resurfacing history as determined from a global impact crater database, *Icarus*, *256*, 78–89.

Kneissl, T., G. G. Michael, T. Platz, and S. H. G. Walter (2015), Age determination of linear surface features using the Buffered Crater Counting approach—Case studies of the Sirenum and Fortuna Fossae graben systems on Mars, *Icarus*, *250*, 384–394, doi:10.1016/j.icarus.2014.12.008.

Matson, D. L., J. C. Castillo-Rogez, G. Schubert, C. Sotin, and W. B. McKinnon (2009), The thermal evolution and internal structure of Saturn's mid-sized icy satellites, in *Saturn From Cassini-Huygens*, edited by M. K. Doughherty, L. W. Esposito, and S. M. Krimigis, pp. 577–612, Springer, Netherlands.

McGill, G. E. (1971), Attitude of fractures bounding straight and arcuate lunar rilles, *Icarus*, *14*(1), 53–58, doi:10.1016/0019-1035(71)90101-1.

Melosh, H. J. (1989), Impact cratering: A geologic process, *Research supported by NASA. New York*, *Oxford University Press* (*Oxford Monographs on Geology and Geophysics*, *No. 11*), *1989*, *253 p.*, *1*.

Moore, J. M. (1984), The tectonic and volcanic history of Dione, *Icarus*, *59*(2), 205–220.

Plescia, J. B. (1983), The geology of Dione, *Icarus*, *56*(2), 255–277.

Plescia, J. B., and J. M. Boyce (1982), Crater densities and geological histories of Rhea, Dione, Mimas and Tethys, *Nature*, *295*(5847), 285–290.

Roatsch, T., R. Jaumann, K. Stephan, and P. C. Thomas (2009), Cartographic mapping of the icy satellites using ISS and VIMS data, in *Saturn From Cassini-Huygens*, edited by M. K. Dougherty, L. W. Esposito, and S. M. Krimigis, pp. 763–781, Springer, Dordrecht, Netherlands, doi:10.1007/978-1-4020-9217-6_24.

Smith, B. A., et al. (1982), A new look at the Saturn system: The Voyager 2 images, *Science*, *215*(4532), 504–537.

Smith, B. A., et al. (1981), Encounter with Saturn: Voyager 1 imaging science results, *Science*, *212*(4491), 163–191.

Smith, M. R., A. R. Gillespie, D. R. Montgomery, and J. Batbaatar (2009), Crater–fault interactions: A metric for dating fault zones on planetary surfaces, *Earth Planet. Sci. Lett.*, *284*(1–2), 151–156, doi:10.1016/j.epsl.2009.04.025.

Stephan, K., R. Jaumann, R. Wagner, R. N. Clark, D. P. Cruikshank, C. A. Hibbitts, T. Roatsch, H. Hoffmann, R. H. Brown, and G. Filiacchione (2010), Dione's spectral and geological properties, *Icarus*, *206*(2), 631–652.

Stevenson, D. J. (1982), Volcanism and igneous processes in small icy satellites, *Nature*, *298*(5870), 142–144.

Tanaka, K. (1982), A new time-saving crater-count technique, with application to narrow features, *NASA Technical Memo*, *NASA TM-85127*, *1*, pp. 123–125 .

Thomas, P. C., et al. (2007), Shapes of the Saturnian icy satellites and their significance, *Icarus*, *190*(2), 573–584, doi:10.1016/j.icarus.2007.03.012.

Wagner, R. J., G. Neukum, B. Giese, T. Roatsch, U. Wolf, T. Denk, and the Cassini ISS Team (2006), Geology, ages and topography of Saturn's satellite Dione observed by the Cassini ISS camera, paper presented at Lunar and Planetary Science XXXVII, Houston, Tex.

Watters, T. R., M. S. Robinson, M. E. Banks, T. Tran, and B. W. Denevi (2012), Recent extensional tectonics on the Moon revealed by the Lunar Reconnaissance Orbiter Camera, *Nat. Geosci.*, *5*(3), 181–185, doi:10.1038/ngeo1387.

Wichman, R. W., and P. H. Schultz (1989), Sequence and mechanisms of deformation around the Hellas and Isidis Impact Basins on Mars, *J. Geophys. Res.*, *94*(B12), 17,333–17,357, doi:10.1029/JB094iB12p17333.

Zahnle, K., P. Schenk, H. Levison, and L. Dones (2003), Cratering rates in the outer solar system, *Icarus*, *163*(2), 263–289.